Synthesis and characterization of Fe3+ doped TiO2 nanoparticles and films and their performance for photocurrent response under UV illumination

(Article begins on next page)

10 November 2024

UNIVERSITÀ DEGLI STUDI DI TORINO

Synthesis and characterization of Fe^{3+} doped TiO_2 nanoparticles and films and their performance for photocurrent response under UV illumination

Kais Elghniji [a], Atef Atyaoui[b], Stefano Livraghi[c], Latifa Bousselmi[b], Elio Giamello[c], Mohamed Ksibi[a]

[a]University of Sfax, *Laboratoire Eau, Energie et Environnement (LR3E), Ecole Nationale d'Ingénieurs de Sfax, BP1173, 3038, Sfax, Tunisia*

[b]Centre de Recherches et des Technologies des Eaux, Technopôle de Borj Cedria B.P. 273, 8020 Soliman, Tunisia

[c]Dipartimento di Chimica and NIS, Università degli Studi di Torino, Via P. Giuria, 7 10125 Torino, Italy

*Corresponding author: Mohamed.Ksibi@tunet.tn

Tel/Fax: +216 74 665 190 (Tunisia)

Abstract
Undoped TiO_2 and Fe^{3+} doped (0.1, 0.3, 0.6 and 1 wt. %) TiO_2 nanoparticles have been synthesized by the acid-catalysed sol-gel method. Iron cations are introduced in the initial solution, before gelification, what promotes their lattice localization. The Fe^{3+} doped TiO_2 films have been fabricated using a dip-coating technique. The effect of iron content on the crystalline structure, phase transformation and grain growth were determined by X-ray diffraction (XRD) Raman spectroscopy, UV–visible diffused reflectance spectroscopy (DRS) and Electron paramagnetic resonance (EPR) spectroscopy. It was demonstrated that all catalysts are composed of mixed-phase crystals of anatase and brookite with anatase as dominant phase. The crystallinity of the brookite and anatase phases decreased with increasing the iron content. The analysis of EPR result further confirms that Fe^{3+} ion are successfully doped in the TiO_2 lattice by substituting Ti^{4+}. It was demonstrated that Fe^{3+} ion in the TiO_2 films plays a role as the intermediate for the efficient separation of photogenerated hole-electron pairs and increases the photocurrent response of the film under UV light irradiation. The maximum photocurrent is obtained on the Fe^{3+} doped TiO_2 film with 0.1% Fe, which is 1.46 times that achieved on undoped TiO_2 film.

1. Introduction
A great deal of effort has been devoted in recent years to develop heterogeneous photocatalysts with good optical-electronic properties. However, TiO_2 catalysts inevitably encounter a serious limit in the following two aspects. A first disadvantage of titania is its high band gap value (3.2eV) which selectively limits its photoactivity to wavelength lower than 387nm. A second limiting factor of the TiO_2 performance is the fast recombination of photogenerated electron-hole pairs. Metal doping is a popular method to improve the photo reactivity of TiO_2 semiconductors under UV-Vis illumination [1-2]. Amongst a variety of metals, iron has been considered an appropriate candidate for incorporation in TiO_2 structure due to the similarity of the ionic radius of Fe^{3+} (0.64 Å) with that of octaedraly coordinated Ti^{4+} (0.68 Å) [3]. It has been also proposed that Fe doping directly influences the intrinsic properties of TiO_2, such as particle size and photocurrent responses under UV light irradiation. The beneficial effect consists in the fact that Fe^{3+} plays a role as intermediate for the efficient separation of photogenerated hole-electron pairs. Fe^{3+} traps photogenerated electrons due to the energy level for Fe^{3+}/Fe^{2+} below the conduction band edge of TiO_2.

2

Simultaneously, Fe^{3+} can trap photogenerated holes due to the energy level for Fe^{4+}/Fe^{3+} above the valence band edge of TiO_2[4,5].

The number of papers on Fe^{3+} doped TiO_2 (iron doped TiO_2) is undergoing an exponential increase. As often occurs in the case of an explosively growing subject, a certain degree of confusion due to conflicting evidence and interpretations is present in the literature. This is mainly due to the variety of synthetic methods adopted to prepare the catalyst [6-11]. Some authors reported the beneficial effect of Fe^{3+} in enhancing electron/hole separation thus increasing the photocatalytic activity [12,14]. As opposite other authors suggested a detrimental effect of Fe^{3+} due to an increase of the rate of charge recombination [15]. To put this controversy into a more realistic and practical catalytic perspective, one study reported that Fe^{3+} doped TiO_2 powder with optimal doping concentration exhibited a greatly enhanced photocatalytic activity in the degradation of isopropanol [16]. Zhu et al [17] have indicated that iron doping of TiO_2 improves photocatalytic activity up to a doping level 0.09% of Fe^{3+}. The concentration of the dopant seems to be the essential factor to determine the potoactivity. In particular the optimum photocatalytic activities can be achieved upon doping at a relatively weak level.

It is well known that titania has three polymorphs in nature: rutile, anatase, and brookite. The two latter phases are metastable at all temperatures and transform commonly to rutile when they are heated. The coexistence of phases in TiO_2 has been suggested to be a factor which reduces the recombination rate of the e^-/h^+ pair [18,19]. As a consequence, an increase in photoactivity seems to be correlated to the coexistence of anatase and brookite phases in TiO_2 [19,20]. Therefore, it is important to understand the effect of the distribution and content of the dopant on phase composition of TiO_2.

The present work aims at complementing such investigations comparing undoped TiO_2 and Fe^{3+} doped TiO_2 nanoparticles and films which are synthesized by the acid-catalyzed sol-gel method. An advantage of the acidic catalysis is that it is possible to enhance simultaneously the crystallization of anatase phase and growth of brookite at low temperature. The influence of Fe^{3+} doping content on both anatase and brookite TiO_2 nanoparticles and the anatase-rutile transformation in the presence of brookite was evaluated. In addition, the photocurrent responses and stability of the Fe^{3+} doped TiO_2 films under a UV-Vis illumination were investigated by amperometric measurement in 0.1 M of NaOH aqueous solution. Our results indicate that Fe^{3+} doped TiO_2 photocatalysts could be an optimal structure for highly sensitive optoelectronic sensors.

2. Materials and methods

2.1. Preparation of Fe^{3+} doped TiO_2 powders

Fe^{3+} doped anatase/brookite TiO_2 powders were synthesized by acid catalyzed sol–gel route. In a typical procedure, a precursor of acidic aqueous solution was prepared by mixing a certain amount of nitric acid with 90 mL of distilled water (pH=2.5) (solution A). 14.8 ml of Titanium tetraisopropoxide $(Ti(OC_3H_7)_4$, Sigma-Aldrich, 97%) were diluted in 80 ml of isopropanol. To this solution, different amounts (1, 0.6, 0.3 and 0.1 %) of $Fe(NO_3)_3 \cdot 9H_2O$ (Sigma-Aldrich, 99.99%) were added according to the required Fe/Ti atom ratio (solution B). Solution A is added drop wise to solution B with constant and vigorous stirring for 24h. The resulting mixture was undergone ageing for 12 h, filtered and washed several times with deionised water. The final product was dried at 50°C during 24 h. The resulting powders were calcined in air at various temperatures for 2h. For comparison, undoped TiO_2 was also prepared by the same procedure without the addition of iron precursor. The Fe^{3+} doped TiO_2 calcined powders are labelled according to their iron content and calcination temperature: $TFe1_t$, $TFe0.6_t$, $TFe0.3_t$, $TFe0.1_t$ and undoped TiO_2 $TFe0_t$, where t means the calcination temperature. For example, $TFe0.6_{500}$ represents the Fe^{3+} doped TiO_2 with Fe/Ti = 0.6% calcined at 500 °C.

2.2. Preparation of Fe^{3+} doped TiO_2 films

The as-prepared powders were used to prepare Fe^{3+} doped anatase/brookite TiO_2 films using a dip-coating technique. TiO_2 films were deposited on a conductive glass plate (area, 4 cm^2). A

well-dispersed suspension (0.4 wt. %) of Fe^{3+} doped TiO_2 powders was prepared in distilled water and stirred for 24 h. A substrate glass plate was coated with TiO_2 by dipping in the TiO_2 suspension, drying under air, and then heating at 120 °C for 30 min. The dip-coating procedure was repeated four times until a thick film of TiO_2 was obtained. The TiO_2 films

were then calcined at a rate of 1 °C min^{-1} up to 400 °C and sintered at this temperature for 30 min.

2.3. Physical-chemical characterization of synthesized solids

The powder X-ray diffraction patterns were recorded at room temperature (using advanced D8, Bruker, Germany): X-ray tube operating at 40 kV and 40 mA, 0.6 mm fixed divergence slits, diffracted beam curved graphite monochromator (Cu $K_{\alpha+1}$ radiation, λ_1= 1.540600 Å, λ_2= 1.544390 Å) and 0.1 mm fixed slit in front of the scintillation detector. The data were collected in the 2θ range 2-70° with a step size of 0.02° and a counting time of 5 s/ step. All peak data measured by XRD analysis were assigned by comparing with those of PCD database. TGA/DTA analysis data were recorded using TG/DTA instrument (Model Pyres Diamond TG/DTA, Perkin Elmer instrument). The temperature ranged from room temperature to 1000°C in order to obtain crystallization and phase-transformation data. All analyses were performed in a flowing air atmosphere of 30 min^{-1} with the heating rate of 20°C min^{-1}. Raman spectra were recorded with a LABRAM HR800 Raman Spectrometer equipped with a He-Ne ion laser emitting at a wavelength of (633 nm). UV-Vis diffuse reflectance (DR UV–Vis.) spectra were recorded by a Varian Cary 5000/UV-Vis.-N.I.R. spectrometer. Electron Paramagnetic Resonance (EPR) spectra were run using a X-band CW-EPR Bruker EMX spectrometer equipped with a cylindrical cavity operating at 100 kHz field modulation. The measurements were carried out in cells that can be connected to a conventional highvacuum apparatus (residual pressure <10^{-6} kPa).

The iron content of the samples was determined using Atomic absorption flame emission spectroscopy AAS (ICE 3000 series). Prior to analyse, fifty milligrams of samples Fe^{3+}doped TiO_2 was transferred into Teflon flask and then completely dissolved in HF-HNO_3 solution (30 /70 % in volume). After dissolution, the mixture was diluted with 100 mL of deionized water and analyzed by (AAS).

2.4. Photo-electrochemical characterization

Photocurrent characterization was performed using a VoltaLab 40 PGZ301 potentiostat (Radiometer Analytical) and VoltaMaster 4.0 software for data acquisition. A 100 ml cell made of quartz was used as photoelectrochemical cell with the Fe^{3+} doped anatase/brookite TiO_2 films as working electrode, a Pt counter electrode and a saturated calomel reference electrode (SCE). All potentials are quoted versus SCE. The geometric surface of the working electrode was 4 cm^2. The electrolyte was an air-saturated aqueous solution with 0.1 M of NaOH. A 150 W Xenon lamp was employed as a UV excitation source (λ=380 nm).

3. Results and discussion

3.1. Determination of iron content

The actual content of Fe^{3+} in different samples was determined by atomic absorption flame emission spectroscopy (AAS). The results are listed in Table 1. It is shown that the actual content of Fe^{3+} measured by AAS is quite close to the theoretical value, indicating that most of Fe^{3+} is inserted in the framework of TiO_2.

3.2. X-ray diffraction patterns of undoped TiO_2 and Fe^{3+} doped TiO_2

Figure 1 shows the evolution of the titania XRD powder spectra as function of the iron loading (calcination T=500°C). The whole pattern is due to the presence of a mixed phase anatase (Pearson's Crystal Data PCD # 1003622) and brookite (2θ~30.8°) (PCD # 1906427) present in all samples including TFe0$_{500}$ with a preponderance of the anatase phase (Table 2). Diffraction peaks due to iron are completely absent in the XRD pattern of the doped iron TiO_2 powder. The absence of peaks due to metal may be attributed to fine dispersion of metal particles on TiO_2 or due to very small metal content [21].

The examination of the diffractograms of the prepared samples indicates that, with increasing

4

iron doping, there is a parallel decrease of intensity of the anatase (101) and brookite (121)

peaks. This phenomenon, more evident for TFe0.6 and TFe1 samples, could arise from the increased surface disorder and/or for the presence of defect sites induced by the iron ions doping [22].

Fig. 2a shows the XRD patterns of TFe1 calcined at different temperatures. It can be observed that acid catalysis enhances the anatase and brookite crystallinity of TiO_2 xerogel dried at 200°C. Anatase and brookite are a metastables TiO_2 polymorphs [23], which are commonly formed at low temperatures in/from solutions. These results are similar to those observed by Yu et al. [24], who synthesized by sol-gel TiO_2 catalysts using acidic (HNO_3) and basic (NH_4OH) catalysis. These Authors claim that the presence of an acidic catalyst enhances the phase transformation of the TiO_2 powders from amorphous to anatase and the growth of brookite phase at 100°C with weight fractions of 65.2 and 34.8%, respectively. In contrast, the NH_4OH not only retards the phase transformation of the TiO_2 powders from amorphous to anatase and from anatase to rutile but also suppresses the growth of brookite phase.

The results in Fig. 2a indicate that the anatase-rutile transition seems to start at 600°C. At this temperature, TFe1 sample is composed of anatase, brookite and a small, but however negligible, fraction of rutile. At 700°C, brookite and anatase phases disappear and the TFe1 powders contain only rutile. It is reported that the formation of Fe_2O_3 and Fe_2TiO_5 would decrease the photoactivity of the photocatalysts because these oxides act as a recombination center of the photogenerated charges [25,26].The formation temperatures of Fe_2O_3 and Fe_2TiO_5 are 600 and 800 °C, respectively [27,28]. In order to fully characterize the crystalline structure of Fe^{3+} doped TiO_2, Rietveld refinement method [29] (considering all peaks in the range of 20–70° (2θ)) was applied on the analysis of XRD data of TFe1$_{800}$ (Fig. 2b). These results confirmed the presence of the only rutile TiO_2 phase. The quality of the agreement between observed and calculated patterns for each phase is measured by a set of factors given by the FULLPROF program. No hint of iron-containing phases such as Fe_2O_3 and Fe_2TiO_5 could be resolved XRD data of TFe1$_{800}$.There are two reasons responsible for this result. A possible reason is that the iron content in the Fe^{3+} doped TiO_2 samples is below the detection limit of this technique whatever the crystal phase formed by iron. Another reason is that $Fe^{3+}$and Ti^{4+} have similar ionic radii (0.79Å versus 0.75 Å), so thus Fe^{3+} can easily substitute Ti^{4+} into TiO_2 lattice [30], as mentioned in introduction section. Based on Hume-Rothery rule, if the difference of atomic radii is less than 15% and the electronegativity of two elements are similar (Fe^{3+}: 1.96, Ti^{4+}: 1.5 [31]), a substitutional solid solution is most likely to be formed. The phenomenon of Fe^{3+} ions doping in TiO_2 crystal satisfies the third of Hume-Rothery rule as well, which states that a lower-valent metal will be soluble in a higher-valent host [32]. Hence, iron ions may substitute titanium ones in the TiO_2 matrix or, alternatively, can be located interstitially forming a Fe^{3+} doped TiO_2 solid solution.

The average crystallite size D_a and D_b of anatase and brookite was estimated according to the Scherrer's equation. The weight fraction of anatase and brookite can be calculated from the following equation [33]:

$W_A = K_A A_A / (K_A A_A + A_R + K_B A_B)$ (1)

$W_B = K_B A_B / (K_A A_A + A_R + K_B A_B)$ (2)

Where, W_A and W_B represent the weight fraction of anatase, brookite and rutile, respectively. A_A, A_B and A_R are the integrated intensity of the anatase (101), brookite (121) and rutile (110) peaks, respectively. The integrated intensity was calculated after correcting for instrumental and wavelength related broadening. $k_A = 0.886$ and $k_B = 2.721$ are two coefficients. There, $A_R = 0$, when rutile peak is not detected.

Usually, the anatase phase of titania is the main product in sol-gel synthesis of TiO_2. However, brookite is also typically present in synthesis products. Brookite can be detected by the appearance of its (121) peak in powder X-ray diffraction patterns at $2\theta \sim 30.8°$. Even if the intensity of the brookite (121) peak is very low compared to the anatase (101) peak, the amount of brookite may be considerable [33-35].

The average crystal size of samples and the contents of anatase and brookite are shown in

Table 2 which shows that the crystallite size of the materials decreases from 13.6 to 11.5 nm with increasing the iron ions content. Such an inhibition of the crystallographic domain growth and phase transformation due to the presence of transition metals inside the TiO_2 lattice is well documented in previous works [36]. In Table 2 it can be also seen that the weight fraction of both phases changes slightly, regardless of the amounts of dopant. This may be attributed to low-level iron doping common to all sample.

3.5. Raman studies

Fig. 3 shows Raman spectra of TFe1 with increasing calcination temperature. At 400°C, the Raman spectrum of anatase shows the six characteristic bands at 144, 197, 399, 513, 519, and 639 cm^{-1}[37]. These peaks can be assigned to the fundamental vibration modes of anatase TiO_2 with the symmetries of E_g, E_g, B_{1g}, A_{1g} and E_g, respectively [38]. The existence of the brookite phase is evidenced in Fig. 3 by the Raman peaks at 216, 243, 284, 320,363 and 450 cm^{-1} [39]. It was also found that the intensity of the bands of brookite and anatase phases became stronger after calcination at 500 and 600°C. The Raman spectra of TFe1 calcined at 700 and 800°C show only the vibrational modes of the rutile phase in agreement with XRD results. The Raman spectra of TFe1 calcined at 500°C (inset) do not present signal at 2940 cm^{-1}ascribed to the presence of the residual organic groups C-H. This could be attributed to the enhanced crystallization degree of anatase phase. No Raman lines due to iron oxide such as Fe_2O_3 and Fe_2TiO_5 are observed in the TFe1 sample when calcined at 700 and 800°C. This is because the iron content of this sample is lower compared with that of the other reports [40,41]. Bickley et al [41] suggested Fe^{3+} ions were well dispersed within the titania matrix at dopant levels up to 1 % iron while at higher levels, segregated pseudo brookite (Fe_2TiO_5) is also formed after calcination at 700 and 800°C.

3.6. UV-Vis diffuse reflectance spectra

The UV-Vis diffuse reflectance spectra of undoped TiO_2 and Fe^{3+} doped TiO_2 samples are depicted in Fig.4. For the undoped TiO_2, the typical absorption edge around 387 nm due to the intrinsic band-gap excitation of anatase (3.2 eV) is clearly visible. Undoped TiO_2 has no absorption in the visible region (>400 nm), whereas Fe^{3+} doped TiO_2 catalysts exhibits both red shifts of the absorption edge and a significant enhancement of light absorption in the range 400-600 nm. Such absorption increases with increasing the iron content in Fe^{3+} doped TiO_2, accompanied by colour changes from white to yellow. According to the literature [42-44], the presence of transition metal ions in TiO_2 introduces new energy levels (Fe^{3+}/Fe^{4+}) into the band gap of TiO_2. Therefore, the visible light absorption in Fe^{3+} doped TiO_2 comes from the electronic transition from the dopant energy level (Fe^{3+}/Fe^{4+}) to the conduction band of TiO_2 [45]. Furthermore, the electronic transition centred at about 500 nm is reported to be due to the d-d transition of Fe^{3+} or to the charge transfer transition between iron ions (Fe^{3+} +Fe^{3+}→Fe^{4+} +Fe^{2+})[45].

3.7. EPR analysis

In Fig. 5 shows the EPR spectra of Fe^{3+}-doped TiO_2 recorded at RT after careful outgassing. EPR is a highly sensitive spectroscopic technique for examining paramagnetic species (levels of Fe^{3+} <0.01% are detectable) and can give valuable information about the lattice site in which paramagnetic Fe^{3+} dopant ions one is located, as reported in previous work both from our laboratory and from other research group [46,47]. Fe^{3+} is a $3d_5$ paramagnetic high spin ion having S=5/2 The interpretation of Fe^{3+} spectra in powders is often difficult due to inhomogeneous broadening, existence of broad and partially overlapping signals and, in particular, because of the role of zero field splitting (ZFS) termes. ZFS parameters (D, E), depend on the strength and symmetry of the crystal field and, when large enough, generate a number of distinct transition in a very large range of magnetic field.

The EPR spectra reported in Fig. 5 are basically composed by two signals. The former is a symmetric line with g factor around 2.0 while the second one, at low magnetic field, is low symmetric and seems composed by various components. Both signals grow in intensity and linewidth, in parallel with the increase of iron loading in the material. It is worth to note that broaden lines due to magnetically interacting iron ions in Fe_2O_3 or other oxides are not

observed in the spectra in agreement with the other results reported in this paper. Moreover the correlation between signal intensity and line width further suggests that iron ions are homogenously diluted in the TiO_2 matrix.

The signal at g=2.0 is typical of trivalent iron in rather symmetric environments (no or very weak zero field splitting with D=E 0) as in the case of Fe^{3+} substituting Ti^{4+} in octahedral symmetry in the anatase structure [48, 49].

The assignment of the low field signals between g=4.75 and g= 4.27 is more difficult. Signals in this magnetic field region are often observed in iron containing materials and are due to Fe^{3+} ions in less symmetric environments causing variations of the zero field splitting term (D, E≠0). This in turn generates a number of transition in a wide spectral range; that at low field only being observed, in X-band EPR spectra. Different possibilities can be invoked, in the case of Fe^{3+} doped TiO_2, to justify a less symmetric environment for the dopant ion. For example, previous EPR works, on rutile samples impregnated with an aqueous Fe^{3+} solution, have assigned the signals at g= 4.75 to isolated high spin Fe^{3+} ions which diffuse to the surface of titania during heat treatment [50,51]. Signals at g factor around 4.3 are also attributed in the literature to the presence of iron cations into an orthorhombic structure such as brookite with highly distorted environment [52-53]. However, we tentatively associate the spectroscopic trend observed in the present work to a partial surface segregation of the iron ions with the annealing process. Note that in the present work, the dopant is mixed from the very beginning with the amorphous gel. The annealing process crystallizes the titanium oxide and promotes the diffusion and segregation of iron to the surface of titania. This assumption is based on the UV–vis results obtained for TFe1 and TFe0.6 calcined at 500°C at. As mentioned above, the UV-vis spectra show an absorption peak at 484 nm which is assigned to the charge transfer transition between iron cations. During the annealing process, a fraction of iron cations can segregate to the surface, thus increasing the probability of observing d-d transition due to Fe^{3+} cations. Summarizing the major fraction of Fe^{3+} is located in octahedral sites of the bulk where it substitutes Ti^{4+} ions. A minor fraction is dispersed, in low coordination sites, at the surface of the solid.
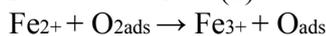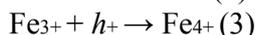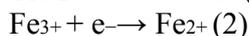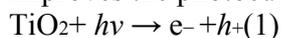
3.8. Photocurrent responses of undoped TiO_2 and Fe^{3+} doped TiO_2 films

The efficiency in the production of photogenerated electron-hole pairs both in undoped TiO_2 and Fe^{3+} doped TiO_2 films was assessed by photocurrent response under UV light irradiation at an applied potential of 0.8 V vs SCE. Fig. 6 shows the typical real time photocurrent response of the Fe^{3+} doped TiO_2 films when the light source is switched on and off, exhibiting rapid photocurrent rise and decay. The dark current density was found to be negligible for all catalysts; however, once light is turned on, a photocurrent is instantaneously generated. In terms of semiconductor physics, when an irradiation provides energy higher than the band gap of TiO_2, the energy excites the electrons from valence band to conduction band and leave a hole in valence band. We have previously shown that the photocurrent is mainly determined by the efficiency of photogenerated hole transfer at the TiO_2/electrolyte and by the electron diffusion to the back contact [54]. The electron-hole is responsible of the photocurrent. When light is turned off, this photocurrent instantaneously decreases to the initial value in the dark, which means that no electrochemical illumination, the maximum photocurrent is obtained for the Fe^{3+} doped TiO_2 film with 0.1%
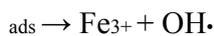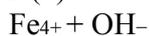
Fe^{3+}, which is 1.46 times that achieved on undoped TiO_2 film. Above this doping concentration, photocurrent decreases. Fe^{3+} therefore has a beneficial effect on photocurrent, it plays a role as the intermediate for the efficient separation of photogenerated hole-electron pairs. Sun et al., have prepared Fe^{3+}-doped TiO_2 nanotube arrays by electrochemical anodization of titanium foil [55]. They suggest that the enhancement of the photocurrent for TiO_2 nanotube arrays is related to the Fe^{3+} dopant. A maximum enhancement of photocurrent response was showed for Fe^{3+}-doped TiO_2 nanotube array film prepared in 0.10M $Fe(NO_3)_3$ + 0.5% HF electrolyte under UV irradiation. The photo-response of this Fe^{3+}-doped TiO_2 film is 1.8-fold higher than that of undoped TiO_2 film. They attribute this result to the effective separation of photogenerated electron–hole upon the substitutional introduction of appropriate

7

Fe^{3+} amount into the anatase TiO_2 structure. However, the beneficial effect is lost and an increase of e^-/h^+ recombination is observed for 1% doping level as the photocurrent is less than the undoped TiO_2.

Fig. 7 shows a schematic illustration of the energy diagram for a Fe^{3+} doped TiO_2 system [56]. A possible mechanism to explain the beneficial effect of Fe^{3+} in TiO_2 is illustrated in the following. The first step is, very likely, the formation of Fe^{2+} species by means of a transfer of photogenerated electrons from TiO_2 to Fe^{3+}(Eq. (2)). The energy level for Fe^{3+}/Fe^{2+} is below the conduction band edge of TiO_2 (0.771V versus normal hydrogen electrode)[57]. According to the crystal field theory [58], Fe^{2+} ion is relatively unstable when compared to Fe^{3+} ion, which have half-filled $3d_5$ orbital. Therefore, the trapped charges can easily release from Fe^{2+} ions and then migrate to the surface to initiate the photocatalytic reaction. Fe^{2+} ions can be oxidized to Fe^{3+} ions by transferring electrons to absorbed O_2 on the surface of TiO_2 (Eq. (4)). Meanwhile, Fe^{3+} can also serve as hole trap (Eq. (3)), due to the energy level for Fe^{3+}/Fe^{4+} (2.20V) above the valence band edge of anatase TiO_2. The Fe^{4+} ions are reduced to Fe^{3+} ions by scavenging electron, while surface hydroxyl group transform into hydroxyl radical(Eq. (5)). These factors inhibit the recombination of photogenerated hole-electron pairs. Therefore, the introduction of an appropriate concentration of Fe^{3+} ions improves the photocurrent responses of photocatalysts.

$$TiO_2 + hv \rightarrow e^- + h^+ \quad (1)$$
$$Fe^{3+} + e^- \rightarrow Fe^{2+} \quad (2)$$
$$Fe^{3+} + h^+ \rightarrow Fe^{4+} \quad (3)$$
$$Fe^{2+} + O_{2ads} \rightarrow Fe^{3+} + O_{ads}^{2-} \quad (4)$$
$$Fe^{4+} + OH^-_{ads} \rightarrow Fe^{3+} + OH \cdot_{ads} \quad (5)$$

This can be attributed to the enhanced crystallinity of anatase phase as Fe^{3+} loading is decreased to 0.1%. The well crystallized anatase might facilitate the transfer of photoelectrons from bulk to surface and thus inhibit their recombination with the photo-generated holes, leading to the enhanced quantum efficiency [59]. In our case the optimal doping concentration is 0.1%. Above this concentration, Fe^{3+} ions play also the role of recombination centers for the photo-generated electrons and holes(Eq. (6), (7) and (8)) and the photocurrent response gradually decreases[60,61]. At doping concentration of 1% this role is preponderant and the photocurrent is strongly decreased.

$$Fe^{4+} + e^- \rightarrow Fe^{3+} \quad (6)$$
$$Fe^{2+} + h^+ \rightarrow Fe^{3+} \quad (7)$$
$$Fe^{2+} + OH \cdot \rightarrow Fe^{3+} + OH^- \quad (8)$$
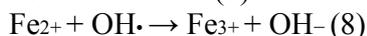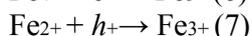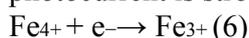
These reactions are in competition with the redox processes that can occur at the solid–liquid interface

4. Conclusion

Undoped TiO_2 and Fe^{3+} doped TiO_2 nanoparticles and films have been prepared by acidcatalyzed sol-gel process. A mixture of anatase and brookite phases with preponderance of anatase is observed in all samples. No crystalline iron phase could be detected. According to XRD measurements, the particle size of anatase decreases with decreasing the iron loading and no hint of iron-containing phases such as Fe_2O_3 and Fe_2TiO_5 could be resolved even after thermal treatments at high temperature. EPR results confirm that Fe^{3+} ions can be successfully inserted into the TiO_2 crystal lattice by substituting Ti^{4+}, thus inducing a small but evident red shift of TiO_2 absorption edge toward visible region. Under UV light irradiation, appropriate Fe^{3+} doping can efficiently separate the photo-generated electrons and holes and consequently improve the photocurrent responses, whereas excess Fe^{3+} induces the recombination of the photo-generated electrons and holes, leading to the decrease of the photocurrent responses. The maximum photocurrent is obtained on the Fe^{3+} doped TiO_2 film with 0.1% Fe, which is 1.46 times that achieved on undoped TiO_2 film.

References

[1] P. Vijayan, C. Mahendiran, C. Suresh, K. Shanthi, Catal. Today. 141 (2009) 220.

[2] R. S. Sonawane, B.B. Kale, M.K. Dongare, Mater. Chem. Phys. 85 (2004) 52.

[3] D.V. Wellia, Q.C. Xu, M.A. Sk, K. H. Lim, T. M. Lim, T. T. Yang Tan, App. Catal A: Gen. 401 (2011) 98

[4] W. Huang, X. Tang, I. Felner, Y. Koltypin, A. Gedanken, Mater. Res. Bull. 37 (2002) 1721.

[5] W. Choi, A. Termin, M.R. Hoffmann, J. Phys. Chem. 98 (1994) 13669.

[6] J. Ovenstone, K. Yanagisawa, Chem. Mater. 11 (1999) 2770.

[7] W.C. Hung, S.H. Fu, J.J. Tseng, H.Chu, T.H. Ko,Chemosphere. 66 (2007) 2142.

[8] J. A. Navío, G. Colón, M. Trillas, J. Peral, X. Domènech, J.J. Testa, J. Padrón, D. Rodríguez, M.I. Litter, Appl. Catal. B 16 (1998) 187.

[9] A. Cabot, A. Dieguez, A. Romano-Rodriguez, J.R. Morante, N. Barsan, Sens. Actuators. B. 79 (2001) 98.

[10] K. Wantala, L. Laokiat, P. Khemthong, N. Grisdanurak, K. Fukaya, J. Taiwan. Inst. Chem. E. 41 (2010) 612.

[11] M.I. Litter, J.A. Navío, J. Photochem. Photobiol. A 98 (1996) 171.

[12] S.W. Lam, K. Chiang, T.M. Lim, R. Amal, G.K.C. Low, J. Catal. 234 (2005) 292.

[13] J. Choi, H. Park, M.R. Hoffmann, J. Phys. Chem. C 114 (2010) 783.

[14] J. Yu, Q. Xiang, M. Zhou, Appl. Catal. B: Environ. 90 (2009) 595.

[15] J.A. Navio, J.J. Testa, P. Djedjeian, J.R. Padron, D. Rodriguez, M.I. Litter, Appl.Catal. A: Gen. 178 (1999) 191.

[16] J.C. Colmenares, M.A. Aramendiá, A. Marinas, J.M. Marinas, F.J. Urbano, Appl. Catal. A Gen. 306 (2006) 120.

[17] J. Zhu, W. Zhang, B. He, J. Zhan, M. Anpo, J. Mol. Catal. A: Chem. 216 (2004) 35.

[18] D.C. Hurum, A.G. Agrios, K.A. Gray, T. Rajh, M.C. Thurnauer, J. Phys. Chem. 107 (2003) 4545.

[19] S. Ardizzone, C. Bianchi, G. Cappelletti, S. Gialanella, C. Pirola, V. Ragaini, J. Phys. Chem. C 111 (2007)13222.

[20] A. Paola, G. Cufalo, M. Addamo, M. Bellardita, R. Campostrini, M. Ischia, R. Ceccato, L. Palmisano, Colloids Surf. A: Physicochem. Eng. Aspects. 317 (2008) 366.

[21] Z. Ambrus, N. Balázs, T. Alapi, G. Wittmann, P. Sipos, A. Dombi and K. Mogyorósi, App. Catal. B: Environ. 18 (2008) 27.

[22] X.H. Wang, J.-G. Li, H. Kamiyama, T. Ishigaki, Thin. Solid. Films. 506 (2006) 278.

[23] Y. Hu, H.L. Tsai, C.L. Huang, J. Eur. Ceram. Soc. 23 (2003) 691.

[24] J. Yu, J. C. Yu, M. K.-P. Leung, W. Ho, B. Cheng, X. Zhao, J. Zhao, J. Catal. 217 (2003) 69.

[25] B. Xin, Z. Ren, P. Wang, J. Liu, L. Jing, H. Fu, Appl. Surf. Sci. 253 (2007) 4390.

[26] Y.H. Zhang, A. Reller, J. Mater. Chem. 11 (2001) 2537.

[27] B. Pal, M. Sharon, G. Nogami, Mater. Chem. Phys. 59 (1999) 254.

[28] J.A. Wang, R.L. Ballesteros, J. Phys. Chem. B 105 (2001) 9692.

[29] R.A. Young, the Rietveld Method, Oxford University Press, New York (1993).

[30] C.Y. Wang, C. Bottcher, D.W. Bahneman, J.K. Dohrman, J. Mater. Chem. 13 (2003) 2322.

[31] Y.C. Cao, T. He, Y. Chen, Y. Cao, J. Phys. Chem. C 114 (2010) 3627.

[32] H. Yamashita, M. Harada, J. Misaka, M. Takeuchi, B. Neppolian, M. Anpo, Catal. Today. 84 (2003) 191.

[33] H. Zhang, J.F. Banfield, J. Phys. Chem. B 104 (2000) 3481.

[34] Y.S. Lin, C.H. Chang, R. Gopalan, Ind. Eng. Chem. Res. 33 (1994) 860.

[35] K.N.P. Kumar, K. Keizer, A.J. Burggraaf, J. Mater. Chem. 3 (1993) 1141.

[36] A.M. Ruiz, A. Cornet, J.R. Morante, Sens. Actuators B. 100 (2004) 256.

[37] T. Ohsaka, J. Phys. Soc. Jpn. 48 (1980) 1661.

[38] K. Mallick, M.J. Witcomb, M.S. Scurrell, Appl. Catal. A: Gen. 259 (2004) 163.
[39] G. Busca, G. Ramis, J.M.G. Amores, V.S. Escribano, P. Piaggio, J. Chem. Soc. Faraday Trans. 90 (1994) 3181.
[40] Z.M. Wang, G. Yang, P. Biswas, W. Bresser, P. Boolchand, Powder. Technol. 114 (2001) 197.
[41] R.I. Bickley, J.S. Lees, R.J.D. Tilley, L. Palmisano, M. Schiavello, J. Chem. Soc Faraday Trans. 88 (1992) 377.

[42] K. Nagaveni, M.S. Hegde, G. Madras, J. Phys. Chem. B 108 (2004) 20204.
[43] T. Umebayashi, T. Yamaki, H. Itoh, K. Asai, J. Phys. Chem. Sol. 63 (2002)1909.
[44] J. Zhu, F. Chen, J. Zhang, H. Chen, M. Anpo, J. Photochem. Photobiol. A 180 (2006) 196.
[45] C. Fàbrega, T. Andreu, A. Cabot, J. R. Morante, J. Photochem. Photobiol. A: Chemistry. 211 (2010) 170.
[46] S. Bordiga, R. Buzzoni, F. Geobaldo, C. Lamberti, E. Giamello, A. Zecchina, G. Leofanti, G. Petrini, G. Tozzola, G. Vlaic, J. Catal. 158 (1996) 486.
[47] F. Turci, M. Tomatis, Isidoro G. Lesci, N. Roveri, B. Fubini, Chem. Eur. J. 17 (2011) 350.
[48] J. Soria, J. C. Conesa V. Augugliaro, L. Palmisano, M. Schiavello, A. Sclafani, J. Phys. Chem. 95 (1991) 274.
[49] M. Graetzel, R.F. Howe, J. Phys. Chem. 94 (1990) 2566.
[50] E.A. Aad, A. Aboukaıs, Catal. Today. 56 (2000) 371.
[51] R. Janes, L.J. Knightley, C.J. Harding, Dyes Pigm. 62 (2004) 199.
[52] R.D. Shannon, J.A. Pask, J. Am. Ceram. Soc. 48 (1965) 391.
[53] R. Arroyo, G. Córdoba, J. Padilla, V.H. Lara, Mater. Lett. 54 (2002) 397.
[54] A. Attyaoui, A. Ben Youssef, L. Bousselmi, Water Science & Technology: Water Supply-WSTWS. 10 (2010) 868.
[55] L. Sun , J. Li, C.L.Wang, S.F. Li , H.B. Chen , C. J. Lin, Sol. Energy Mater. Sol. Cells. 93 (2009) 1875.
[56] J. Lei, X. Li, Int. J. Hydrogen Energy 36. (2011) 8167.
[57] Y. Ma, X.T. Zhang, Z.S. Guan, Y.A. Cao, J.N. Yao, J. Mater. Res. 16 (2001) 2928.
[58] M.H. Zhou, J.G. Yu, B. Cheng, J. Hazard. Mater. 137 (2006) 1838.
[59] H.C. Choi, Y.M. Jung, S.B. Kim, Vib. Spectrosc. 37 (2005) 33.

[60] T.Z. Tong, J.L. Zhang, B.Z. Tian, F. Chen, D.N. He, J. Hazard. Mater 155 (2008) 572.
[61] A. Kudo, H. Misek, Chem. Soc. Rev. 138 (2009) 253.

Fig.1. X-ray powder diffraction spectra of Fe^{3+} doped TiO_2 and undoped TiO_2 samples calcined at 500 °C. The peaks marked **a** and b represents the anatase and brookite, respectively.

Fig.2.(a)X-ray powder diffraction spectra of TFe1 sample calcined at different temperatures; (b) Rietveld plot for TFe1sample calcined 800°C, **a, r** and **b** are denoted anatase, rutile and brookite TiO_2, respectively.

Fig.3. The Raman spectra of TFe1 calcined at 400°C, 500°C, 600°C, 700°C and 800°C. r and b represents rutile and brookite. Inset shows the Raman spectra of TFe1 calcined at 500°C

Fig. 4. UV-Visible diffused reflectance spectra of undoped TiO_2 and Fe^{3+} doped TiO_2 sample calcined at 500°C.

Fig. 5.EPR spectra of Fe^{3+} doped TiO_2 samples calcined at 500°C

Fig. 6: The effect of the doping of Fe^{3+} in TiO_2 on the photocurrent response with UV illumination

Fig. 7 Schematic diagram illustrating the charge transfer from excited TiO_2 to the different states of Fe^{3+} ions; C_B and V_B refer to the energy levels of the conduction and valence bands of TiO_2, respectively [52].
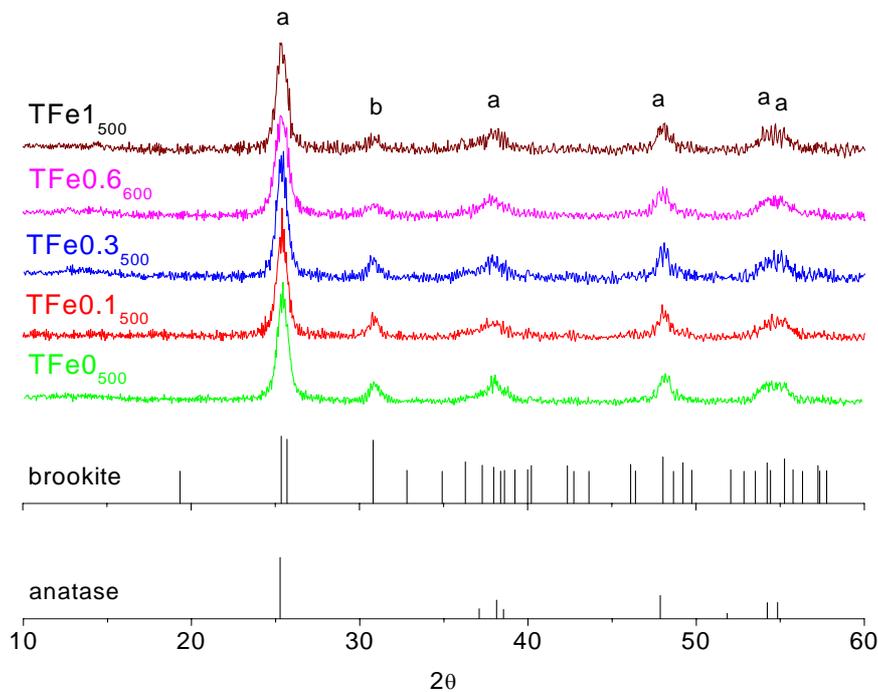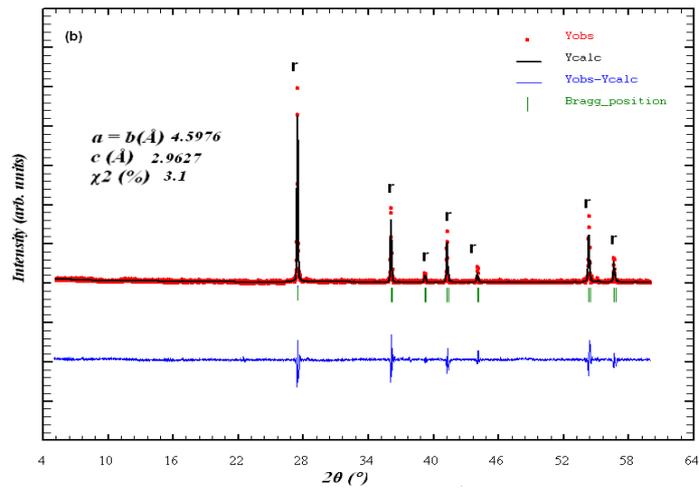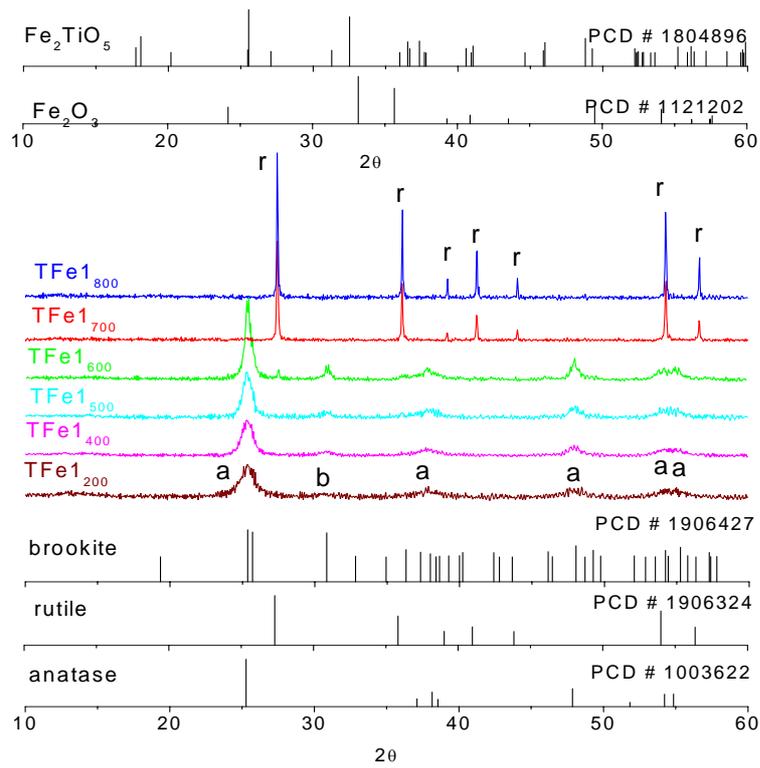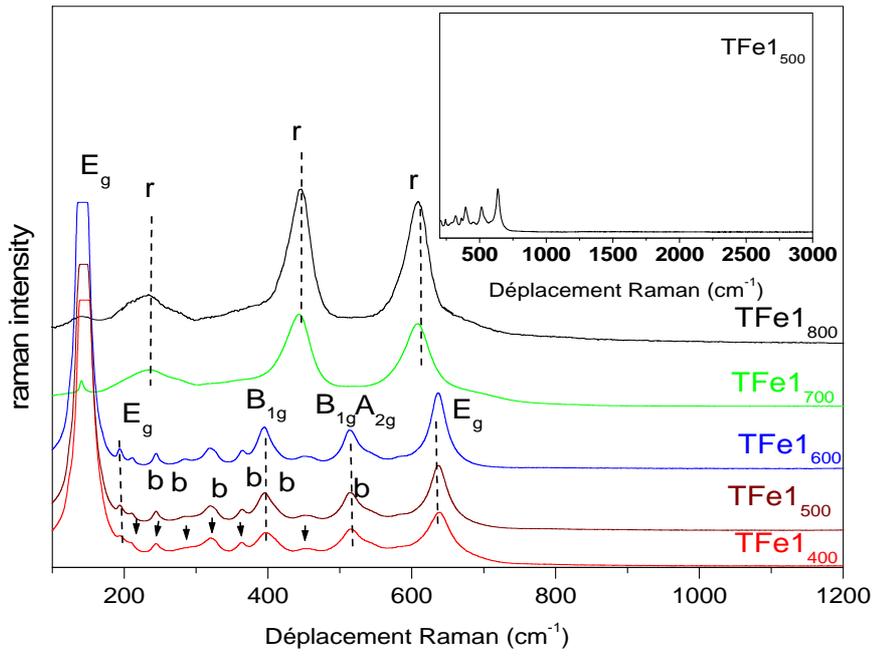

Figure 1

Figure 2

Figure 3
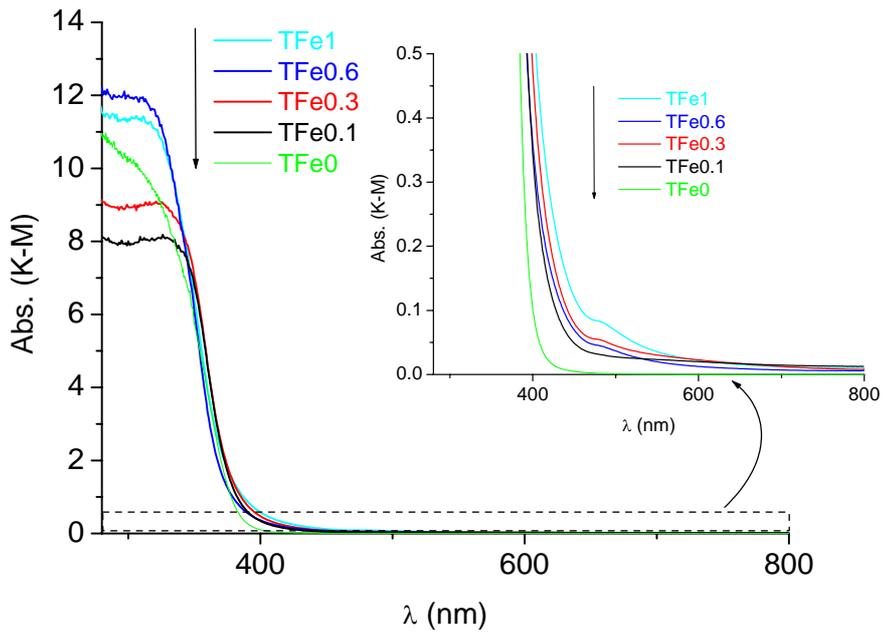
Figure 4
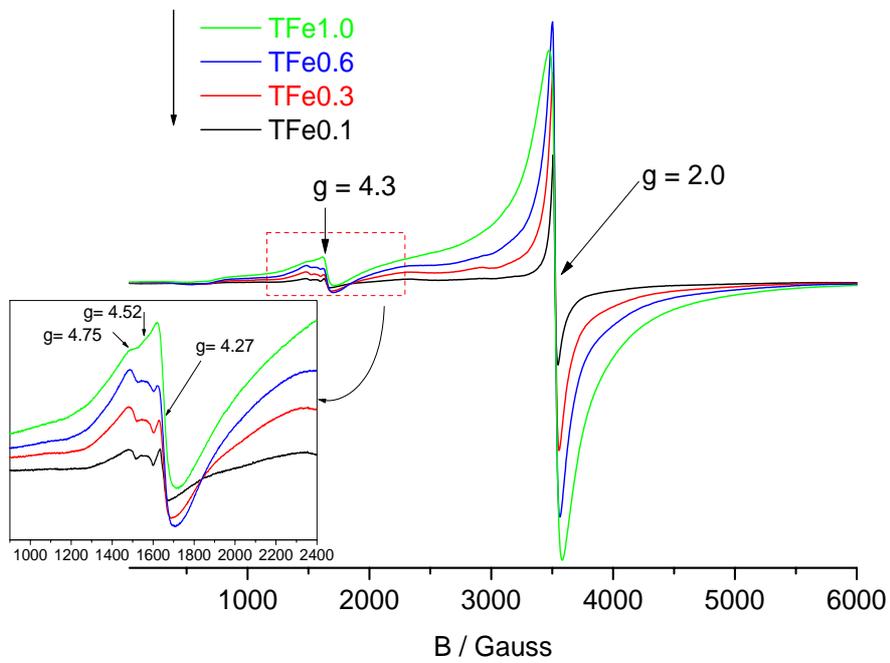
Figure 5

Figure 6

Figure 7

14
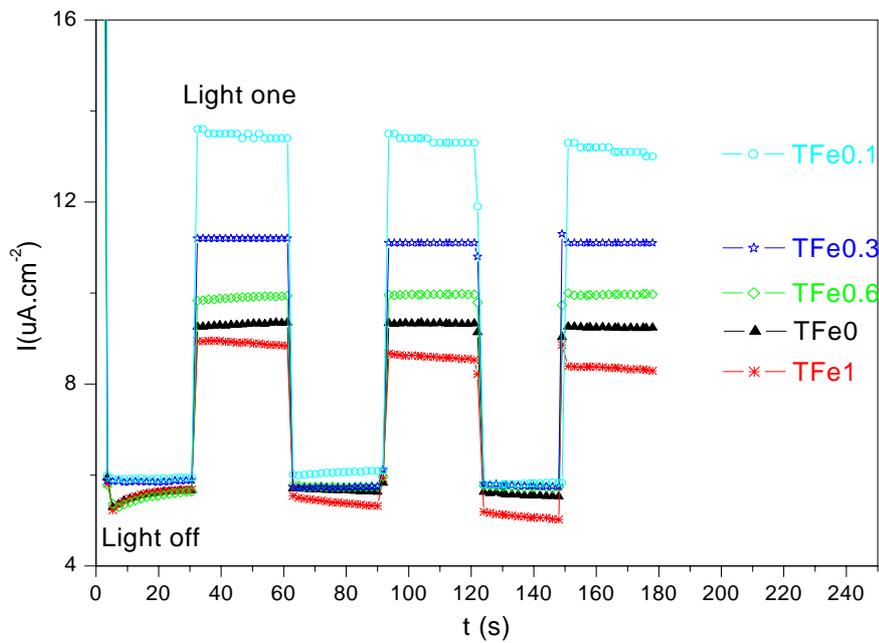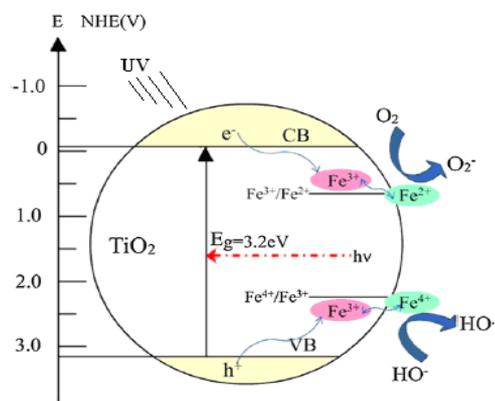
Table 1. Iron contentin Fe^{3+}doped TiO_2 samples obtained from (AAS).

Sample	Calculated Fe content (%)	(AAS) Fe content (%)
TFe1	1	0.82
TFe0.6	0.6	0.47
TFe0.3	0.3	0.26
TFe0.1	0.1	0.098
TFe0	n.d	n.d

Table 2 Phase composition and crystalline size of Fe^{3+}doped TiO_2 samples as function of iron content (500 °C) and calcined (TFe1) at different temperatures.

Sample	[a]Phase composition		[b]Crystallite size (nm)	
			D_a	D_b
$TFe1_{200}$	A (73%)	B (27%)	6.5	8.7
$TFe1_{400}$	A (73%)	B (27%)	9	14.5
$TFe1_{500}$	A (72.5%)	B (27.5%)	11.5	20.3
$TFe0.6_{500}$	A (72.4%)	B (27.6%)	12.5	21
$TFe0.3_{500}$	A (72.1%)	B (27.9%)	13	22.7
$TFe0.1_{500}$	A (72.6%)	B (27.4%)	13.6	22.1
$TFe0_{500}$	A (71.8%)	B (28.2%)	13.66	21.8

[a] Phase composition is defined as the ration between the two main peaks area of anatase (A) and brookite (B) phase.

[b] Particle size was calculated with Scherrer equation by using the (101), (110) and (211) peaks appearing of anatase, rutile and brookite respectively.